Structure and mechanics of aegagropilae fiber network

Gautier Verhille[a,1], Sébastien Moulinet[b], Nicolas Vandenberghe[a], Mokhtar Adda-Bedia[c], and Patrice Le Gal[a]

[a]Aix Marseille Université, CNRS, Centrale Marseille, Institut de Recherche sur les Phénomènes Hors Equilibre, 13013 Marseille, France; [b]Laboratoire de Physique Statistique, Ecole Normale Supérieure, Université Pierre et Marie Curie Paris 06, Université Paris Diderot, CNRS, 75005 Paris, France; and [c]Université Lyon, Ecole Normale Supérieure de Lyon, Université Claude Bernard, CNRS, Laboratoire de Physique, F-69342 Lyon, France

Edited by David A. Weitz, Harvard University, Cambridge, MA, and approved March 20, 2017 (received for review December 19, 2016)

Fiber networks encompass a wide range of natural and manmade materials. The threads or filaments from which they are formed span a wide range of length scales: from nanometers, as in biological tissues and bundles of carbon nanotubes, to millimeters, as in paper and insulation materials. The mechanical and thermal behavior of these complex structures depends on both the individual response of the constituent fibers and the density and degree of entanglement of the network. A question of paramount importance is how to control the formation of a given fiber network to optimize a desired function. The study of fiber clustering of natural flocs could be useful for improving fabrication processes, such as in the paper and textile industries. Here, we use the example of aegagropilae that are the remains of a seagrass (*Posidonia oceanica*) found on Mediterranean beaches. First, we characterize different aspects of their structure and mechanical response, and second, we draw conclusions on their formation process. We show that these natural aggregates are formed in open sea by random aggregation and compaction of fibers held together by friction forces. Although formed in a natural environment, thus under relatively unconstrained conditions, the geometrical and mechanical properties of the resulting fiber aggregates are quite robust. This study opens perspectives for manufacturing complex fiber network materials.

fiber network | fiber aggregation | *Posidonia oceanica* | fibrous material

Aegagropilae are a natural aggregate of fibers produced by the decomposition of leaves and roots of *Posidonia oceanica*. The fibers are entangled by sea motion until the clusters reach the shore (1) (Fig. 1). *P. oceanica* is an endemic plant of the Mediterranean Sea with very long and thin leaves (about 1-m long, 1-cm wide, and less than 1-mm thick). The name aegagropilae originates from the Greek [αίγαγρος (wild goat) and πῖλος (fur)] and refers to the resemblance between the shape of these balls and those regurgitated by goats. Natural fiber clustering occurs for different species of aquatic plants, such as the so-called seaballs that can be found on the Atlantic Ocean and lake shores (2, 3).

P. oceanica meadows play an important ecological role in the preservation of Mediterranean coasts. They constitute plant barriers that promote sediment trapping and oxygen production in seabed, and the accumulated remains protect the beaches from erosion. Moreover, aegagropilae fibers are suitable materials for insulation in construction and automotive industries. After submitting them to various tests, they recently landed in the marketplace under the name of Neptutherm. Beyond the curiosity that these natural objects can provoke, aegagropilae samples found on beaches raise several fundamental questions. The first set of questions is on their formation process. How can fibers be entangled and packed by a flow without any confinement? How long does it take to form a cluster? Can one explain the size distribution of these aggregates? The second set of questions is on the cohesion of these structures. How can we relate the apparent stiffness of these balls to the interaction of the fibers and the topological properties of the network?

Natural and manmade fiber networks are abundant structures and arise on a wide range of length scales. Examples may be found in both biological systems, such as the cytoskeleton of a cell (4), blood clots (5), and biological tissues (6), and technology, such as nanotube bundles (7), paper (8), textiles, and felts (9–11). The mechanical response of fiber assemblies depends on both the properties of the elementary thread and the density, connectivity, and ordering of the network. Therefore, the functional properties of these materials can be tuned by controlling their formation processes. The manufacturing of some athermal networks, such as paper, involves transport of fibers in a fluid flow (8). During this process, fibers are advected and deformed elastically, and they interact through interfiber friction (12, 13). From this perspective, aegagropilae are an archetype of these fiber networks, and understanding the clustering mechanism can shed light on the fundamental aspects of fiber aggregation dynamics. Here, we perform various measurements on aegagropilae to characterize their structural and mechanical properties. Our observations provide a qualitative understanding of the formation process of this fiber network.

Structural Properties of Aegagropilae

Aegagropilae were collected at two different locations of the Mediterranean shore: at Six Fours, France (43°06′03″ N, 5°49′20″ E) and on Porquerolles Island, France (43°00′02″ N, 6°13′38″ E) with the authorization of Port-Cros National Park. On the first beach, nearly 2,000 samples were collected to determine their size and mass distributions. To avoid any bias in the sampling caused by damage of aegagropilae by human activity, all samples were collected on a morning in winter, the day after a storm. Moreover, only balls found at a distance less than 10 m from the sea were collected, assuming that the ones located farther away from the sea might have been released by a precedent storm. At the second spot, few samples were picked up in seabed to investigate the geometrical and mechanical properties of fiber

Significance

Aegagropilae are centimeter-sized, nearly spherical fiber aggregate found on Mediterranean beaches. They result from aggregation and compaction of the remains of the seagrass *Posidonia oceanica*. We find that they possess remarkable mechanical properties, which are unexpected for a structure formed by random agitation caused by sea motion and held together solely by friction between the fibers. The study of such material offers perspectives for complex materials, such as felts and insulation materials.

Author contributions: G.V., S.M., N.V., M.A.-B., and P.L.G. performed research, analyzed data, and wrote the paper.

The authors declare no conflict of interest.

This article is a PNAS Direct Submission.

[1]To whom correspondence should be addressed. Email: gautier.verhille@irphe.univ-mrs.fr.

This article contains supporting information online at www.pnas.org/lookup/suppl/doi:10.1073/pnas.1620688114/-/DCSupplemental.

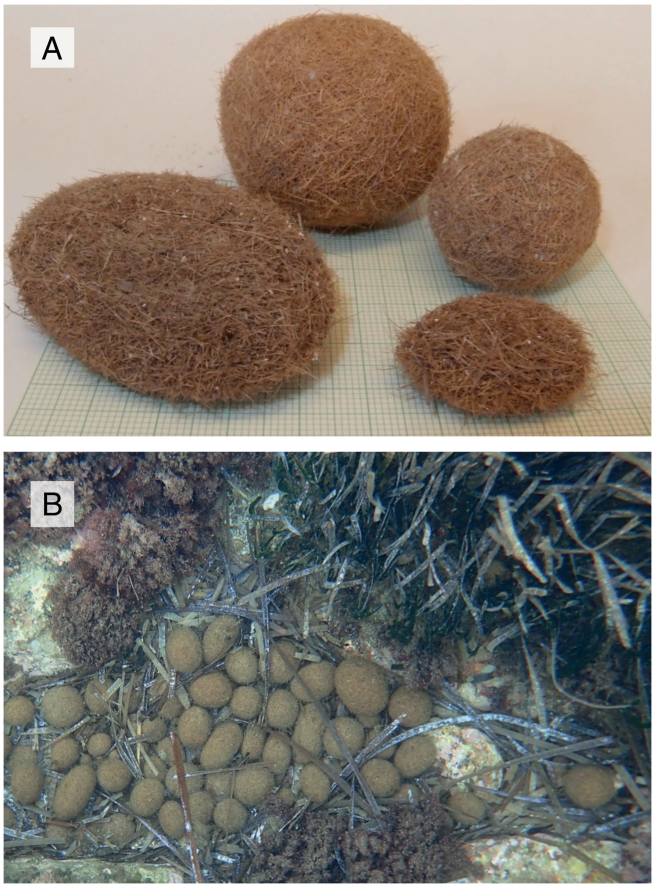

Fig. 1. Aegagropilae formed from aggregation of *P. oceanica*. (*A*) Samples of aegagropilae of various shapes and sizes collected on the beach and placed on millimeter paper. (*B*) Aegagropilae trapped in the seabed at the verge of a *Posidonia* meadow (top right) located at 2-m depth and 20 m from the shore.

aggregates and the influence of aging and drying on cluster compaction.

Mass and Size. The set of 2,000 samples was dried at room temperature for 2 wk to remove the water trapped inside the aggregates. Then, the mass of each aegagropila was measured using an analytical balance (MXX-123; Denver Instrument) with a resolution of 1 mg. Approximating the balls with ellipsoids of revolution (Fig. 1), we have measured the length of their principal axes a, b, and c ($a>b>c$) by fitting with ellipses images taken from the top and the side.

The scatterplot of mass as a function of volume of all collected samples is reported in Fig. 2*A* and shows that their densities are distributed around the average density. This result confirms that the mass and volume of the aggregates are correlated positively. Moreover, the probability density functions (pdfs) of the mass and size have been computed and superimposed on a log-normal probability distribution $P(x)$ given in ref. 14:

$$P(x) = \frac{1}{x\sigma\sqrt{2\pi}} e^{-\frac{(\log x-\mu)^2}{2\sigma^2}}, \qquad [1]$$

where the parameters μ and σ were determined from the measured mean and variance of the corresponding distribution, respectively (Table 1). Fig. 2 *B* and *C* shows that both mass and size distributions are accurately represented by log-normal laws. The distributions of the diameters show a predominance of prolate spheroidal shapes: the geometric mean of a is twice as large as those of b and c (Fig. 2*D* and Table 1). Moreover, as evidenced by the values of SD in Table 1, the dispersion of the data is approximately equal for all lengths. This result suggests the existence of a "state variable" that selects both geometry and mass distributions of the aggregate and allows for a positive correlation between size and mass of the aggregates (in agreement with Fig. 2*A*). Indeed, Eq. **1** shows that linear transformations of the variable x preserve both log-normal behavior and the geometric SD. The formation process of the aggregate could be the underlying mechanism that provides such a state variable and in turn, controls size and mass distributions of aegagropilae.

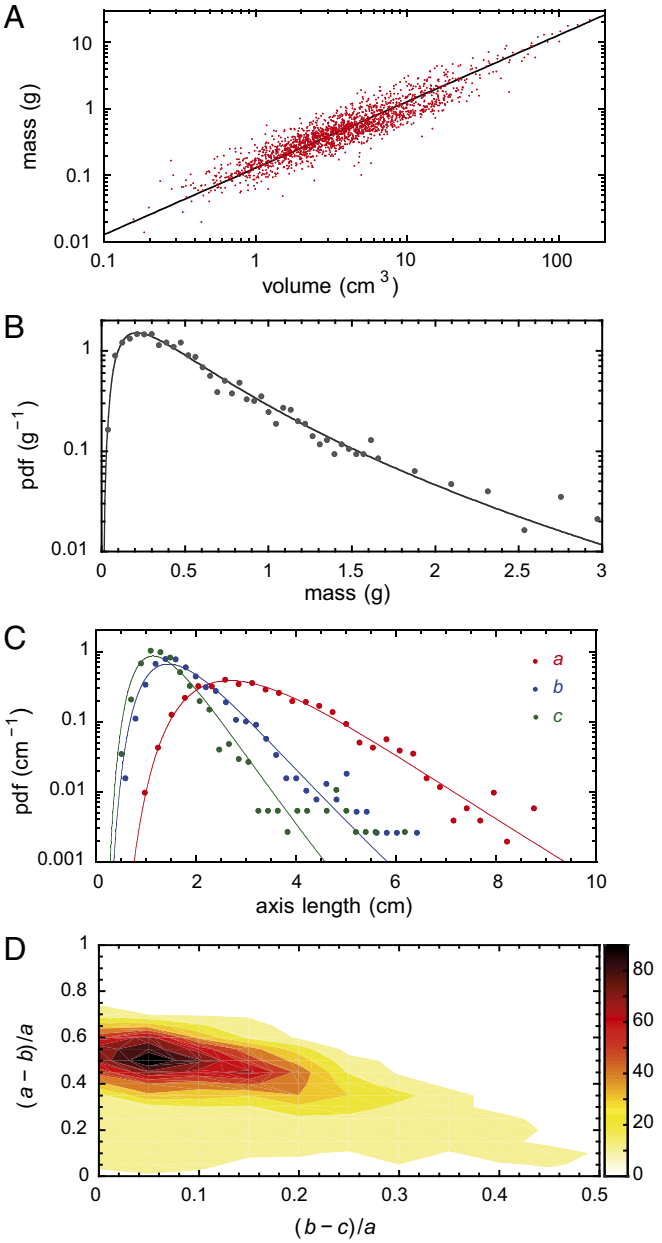

Fig. 2. (*A*) Scatterplot of mass vs. volume of the collected balls. The solid line denotes an average density of 128 kg m^{-3}. (*B* and *C*) The pdfs of the mass of aegagropilae and the main axes of the ellipsoid that characterizes their shapes (details are in the text). Dots represent experimental data, and solid lines are the corresponding log-normal distributions with parameters μ and σ given in Table 1. (*D*) 2D histogram of the aspect ratios $(a-b)/a$ and $(b-c)/a$, showing that the most probable shape is a prolate ellipsoid of revolution with $b \simeq 0.50a$ and $c \simeq 0.45a$.

Table 1. Geometric mean (e^{μ}) and geometric SD (e^{σ}) of the actual distributions

x	Mean	SD
Mass (g)	0.212	1.458
a (cm)	2.681	1.436
b (cm)	1.449	1.47
c (cm)	1.146	1.458

Log-normal distributions arise in the description of many phenomena that involve either growth or division mechanisms. Examples may be found in nature, social sciences, technology, biology, and medicine (15–19). The reason is that, for many natural processes of growth, relative growth rate is independent of size (16). Moreover, hierarchical processes in fragmentation are known to end up with a log-normal distribution of the fragment sizes (15). The question of whether aegagropilae fiber networks are generated by a division or a growth process arises. If growth is the underlying mechanism, the evolution of the mass $m(t)$ of the aggregate would obey the following equation:

$$\frac{\mathrm{d}m}{\mathrm{d}t} = k(t)m(t), \qquad [2]$$

where $k(t)$ is a relative growth rate that is generally independent of size but may evolve in time (16). Eq. **2** can be rewritten as

$$\log \frac{m(t)}{m_0} = \int_0^t k(t')\mathrm{d}t', \qquad [3]$$

where m_0 is an initial mass from which growth proceeds. Because $k(t)$ may fluctuate randomly in time because of external forces acting on the cluster (flow, topography of the seabed ...), the mass $m(t)$ is log-normally distributed if the central limit theorem can be applied on the distribution of $k(t)$.

Eq. **3** shows that this formation process needs a nucleus from which growth initiates. We have disentangled hundreds of samples and indeed, found inside some of them rhizome fragments (20%) and foreign bodies (plastic, textile, wood fragments ...; 20%) that may serve as an initial seed for aggregation. Nonetheless, it is worth noticing that most of the samples (60%) do not present any specific seed, indicating that aggregation may initiate without external nucleus (20, 21). Therefore, the log-normal behavior of the probability distributions of mass and size is not sufficient to unravel aegagropilae formation process and discriminate between fragmentation and growth mechanisms.

X-Ray Tomography. To characterize the internal structure of aegagropilae, we performed X-ray tomography on several samples collected on the beach with a resolution of 18 μm and studied their density distributions and fiber orientations. Fig. 3*A* displays an example of the equatorial section of a nearly spherical sample (the complete tomography is shown in Movie S1). In addition, we performed a tomography on a ball collected underwater and kept inside a water container; then, a second tomography was made on the same ball after it dried. The structural properties of this sample were similar to balls collected on the beach, and neither size nor concentration field have been significantly distorted during drying. The result that all clusters share the same qualitative features confirms that the structural properties of aegagropilae are inherited during their formation in the seabed.

Fig. 3*B* shows that the distribution of fibers in the aggregate is inhomogeneous. The fiber concentration increases quadratically with the distance to the center and reaches a maximum in the vicinity of the border. Similar concentration fields, with a dense shell surrounding a loose core, are observed when slender elastic objects are tightly confined, such as a thin sheet crumpled into a ball (22, 23) or a long steel filament packed in a container (24). In these cases, the process of packing involves forces applied on the external surface of the folded object. The similarity of the density distributions suggests that a comparable compaction mechanism takes place after the aggregate has been already formed.

Moreover, fiber orientation is accessible from the tomography of aegagropilae by fitting a virtual cylinder (length of 270 μm and diameter of 36 μm) inside the full 3D image of a fiber aggregate. This operation is performed around each voxel, with the gray level indicating that it belongs to a fiber. The orientation is then characterized by the angle $\phi \in [0, \pi/2]$ between the axis of the cylinder and a line joining this voxel to the center of the mass of the sample (Fig. 3*A*). To probe any effect of the inhomogeneous density distribution on fiber orientation, we focused our study on two regions: the "core" (around the center of mass) and the "crust" (dense shell near the surface) of the aggregate. In the example reported here, Fig. 3*C* (Fig. 3*D*) shows the orientation distribution in a core (crust) for which $r \lesssim 6.8$ mm

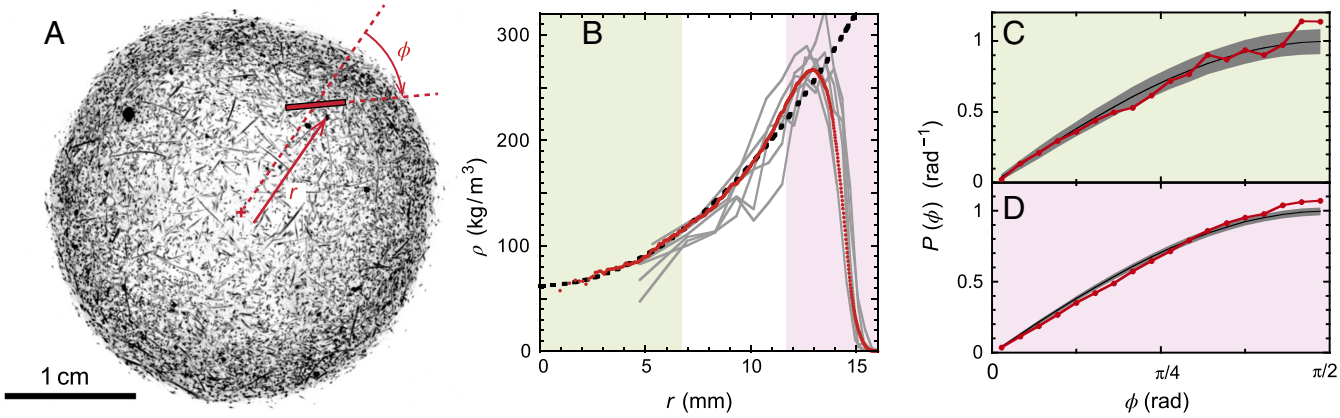

Fig. 3. Results of X-ray tomography for nearly spherical aegagropilae of radius $R \approx 15$ mm and mass 2.56 g. (*A*) A typical tomography image (here at the equator of the sphere). In red is a sketch of the definition of the distance r to the center of mass and the angle ϕ between a fiber and the radial direction. (*B*) Local density $\rho(r)$. The red curve is obtained by integrating over the whole solid angle of the sphere. Gray curves are obtained for six different conical sectors with a 20° summit angle. The black dashed curve is a quadratic fit $\rho(r) = \rho_0(1 + \alpha r^2)$ of the measured local density for $r \leq 10$ mm. (*C* and *D*) The pdfs of the orientation ϕ in the core and crust region represented in *B* by green and pink, respectively. The black curves show the function $P(\phi) = \sin\phi$ expected for a statistically homogeneous distribution. The widths of the gray areas are the SDs σ for a random sampling over the same number of fibers detected in the region. Because the crust is denser than the core, σ is smaller in *D* than in *C*.

($r \gtrsim 11.7$ mm) compared with a homogeneous orientation distribution. Although fiber orientations in the core are found to be isotropic, within the fluctuations expected at this density, the distribution in the crust shows an excess of orthoradial fibers, but the deviation from the isotropic distribution remains very weak. Such features are also observed with sheets or filaments packed in a container (23, 24). These observations suggest that aegagropilae are formed by aggregation of randomly oriented fibers followed by a compaction of the resulting floc, probably caused by sudden changes in sea motion.

Fiber Properties. The connectivity and mechanical response of aegagropilae depend on the nature of their constituent fibers. To this purpose, we visually analyzed *Posidonia* fibers using SEM images near the surface of the aggregate. A typical example is shown in Fig. 4*A*, in which one observes that the fibers are slender objects with a typical cross-section of 100-μm width. Except for the presence of small asperities on the fibers made of salt crystals formed during the evaporation of sea water, the fiber surface is relatively smooth. Fig. 4*A* also shows that a few fibers have broken into a disordered bundle of smaller fibers. However, these fibers are mainly localized at the surface, and their damage is probably caused by the action of the surrounding environment (e.g., during their transport to the shore). Therefore, it is unlikely that these scarce asperities play a role in the formation process or influence the contact behavior between fibers.

To further characterize the individual fibers, we carefully disentangled a seaball of size $32 \times 15 \times 14\ \mathrm{mm}^3$ by avoiding fiber breakage during the separation process and measured lengths L and curvatures κ. Fibers were extracted both near the surface of the seaball (324 fibers) and deeper inside it (340 fibers). No difference in fiber morphology was detected between the two samples. We also analyzed in situ 40 fibers from X-ray tomography and found similar properties. The pdf of fiber lengths reported in Fig. 4*B* shows a large distribution that ranges from 0.5 to 20 mm with a predominance of short fibers and a weighted average length $\langle L^2 \rangle / \langle L \rangle = 7.7$ mm. Moreover, we measured the maximum deflexion Δ of each fiber and estimated its typical curvature as $\kappa \approx \Delta / L^2$. Our results show that most fibers satisfy $\kappa L \lesssim 0.5$.

Therefore, the constituent fibers can be considered as straight slender objects with a geometric aspect ratio close to 80 and lengths smaller than the seaball characteristic size. Our measurements show that fiber self-entanglement is unlikely and suggest that the cohesion mechanism within aegagropilae is dominated by fibers elasticity and frictional contacts between them. As observed in wool felts (11) or artificial aggregates (20), these two ingredients are sufficient to make stable and cohesive spherical flocs.

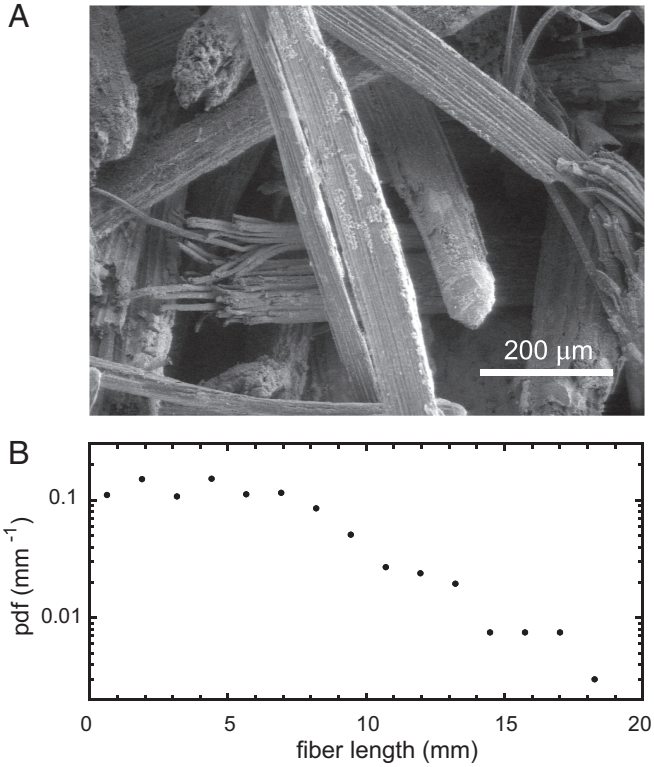

Fig. 4. Morphology of individual fibers. (*A*) SEM image of fibers close to the surface of aegagropilae. (*B*) The pdf of fiber lengths obtained from a disentangled seaball. The weighted average length of the distribution $\langle L^2 \rangle / \langle L \rangle$ is 7.7 mm.

Mechanical Properties of Aegagropilae. The dense structure of aegagropilae provides them with a high stiffness: some balls can resist finger pressure. To quantify this feature, balls were indented using a stainless steel bead of radius $R_{\mathrm{ind}} = 2.3$ mm. The position δ of the indenter is controlled by a translation stage, and a dynamometer allows for the measurement of the reaction force F experienced by the indenter with an accuracy of 10^{-3} N. A typical experiment consists of approaching the indenter until it touches the sample ($\delta = 0$), loading it over a depth δ_{max}, and then unloading it. To probe the mechanical response of the crust region only, the maximum displacement is fixed to 5% of the size of the ball, which also allows us to satisfy $\delta_{\mathrm{max}} \ll R_{\mathrm{ind}}$ for all studied balls. A typical curve $F(\delta)$ is displayed in Fig. 5*A* and shows a hysteresis between loading and unloading cycles: during the first stage of unloading, the force abruptly decreases, and the contact is lost at a position $\delta \neq 0$, indicating a permanent irreversible deformation.

The material response of aegagropilae is probed at relatively small strains: for a displacement $\delta \ll R_{\mathrm{ind}}$, the radius of the contact area is $a \approx \sqrt{2\delta R_{\mathrm{ind}}}$, and the typical strain is then $\epsilon \sim \delta / a \approx \sqrt{\delta / 2R_{\mathrm{ind}}}$. For a typical displacement $\delta = 500$ μm, one has $\epsilon \approx 0.3$. Therefore, the elastic response of the ball can be assumed to be linear, and the force $F(\delta)$ is expected to follow a Hertzian contact law: $F(\delta) \propto \delta^{3/2}$. This assumption is confirmed experimentally (Fig. 5*A*) and allows us to estimate an effective Young modulus E of the fibrous material using ref. 25:

$$F = \frac{4}{3} E R_{\mathrm{ind}}^{1/2} \delta^{3/2}. \qquad \textbf{[4]}$$

Eq. **4** applies for elastic materials with zero Poisson ratio, a property that is often encountered in hollow materials (26). This property is confirmed for the studied samples, because no measurable lateral expansion was detected during indentation. Fig. 5*B* summarizes the moduli measured for 26 different samples as a function of their mean density. The results are quite dispersed: even on a single sample, Young moduli measured at different points can vary by a factor of three. This variability confirms the disparity of the samples and the inhomogeneity within a given ball as expected from a random natural process. Nevertheless, Fig. 5*B* shows a trend of a Young modulus E to scale as $\bar{\rho}^3$, where $\bar{\rho}$ is the mean density of the ball. Such a behavior relating the elasticity of the network and its density occurs generically in the mechanics of fiber aggregates (27, 28) within the assumption that the network responds to applied small deformations by storing elastic energy in the fibers without major topological reorganization.

The structural study of aegagropilae is consistent with a cohesion ensured by interfiber contacts. Therefore, one can assume that the fiber aggregate is a 3D assembly of slender rods of typical length L, diameter d, and bending stiffness $B_f \sim E_f d^4$. The

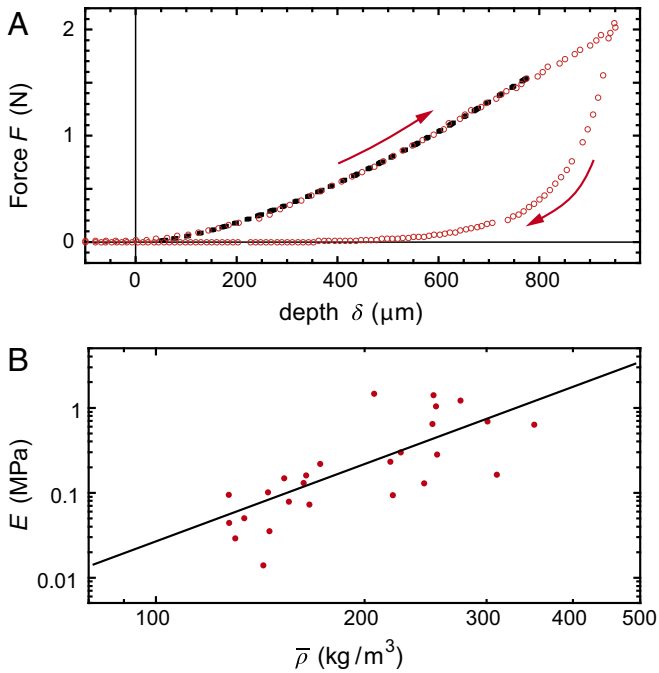

Fig. 5. Mechanical response of a seaball. (*A*) Indentation curve $F(\delta)$ of a seaball of mass 2.95 g and mean density of 275 kg m^{-3}. The dashed line is a fit $F \propto \delta^{3/2}$ law expected for a Hertzian contact. Using Eq. **4** yields a Young modulus $E = 1.16$ MPa. (*B*) Young moduli of the studied aegagropilae as function of their mean density $\bar{\rho} = 6m/\pi abc$. The gray line is $E \propto \bar{\rho}^3$ power law fit.

resulting network is characterized by a coordination number N_c (average number of contacts on a fiber) and a typical distance between contact points on a fiber $\ell \sim L/N_c$. At the level of one fiber, the bending energy associated with a transverse displacement δ is $U_f \sim B_f(\delta/\ell^2)^2 L$. To compute the effective modulus E of the assembly, the standard form of the elastic energy of a homogeneous body $U = E(\delta/\ell)^2\Omega$, where Ω is a given volume, should be balanced with the bending energy nE_f of n fibers within this volume. Using $n \sim \phi\Omega/(d^2L)$, where ϕ is the volume fraction, the effective modulus writes

$$E \sim E_f\phi\left(\frac{d}{\ell}\right)^2 \sim E_f\phi\left(\frac{N_c d}{L}\right)^2. \quad [5]$$

The coordination number N_c is a key quantity to estimate the mechanical properties of the fiber network. For an assembly of randomly oriented slender rigid fibers, one finds $N_c = 2\phi L/d$ (27, 29), and the linear behavior with ϕ seems to be a robust result (30). Substitution in **5** yields the simple scaling $E \sim E_f\phi^3$. Moreover, assuming that the volume fraction of a seaball is well-approximated by $\phi = \bar{\rho}/\rho_f$, with ρ_f being the density of the elementary fibers, one deduces the scaling behavior (27)

$$E \sim E_f\left(\frac{\bar{\rho}}{\rho_f}\right)^3, \quad [6]$$

which is in agreement with experimental results in Fig. 5*B*. Although a detailed analysis on a model system is certainly needed to reach a better insight, it is worth comparing the order of magnitude of the predicted effective modulus with the measurements in Fig. 5*B*. Using a typical Young modulus $E_f = 1$ GPa and (the measured) $\rho_f = 1.4 \times 10^3$ kg m^{-3}, one finds that a prefactor of order 0.1 in the scaling law (6) enables us to achieve correctly the order of magnitude of the experimentally measured Young moduli.

The previous modeling addressed the stiffness of aegagropilae during a loading cycle and for small applied deformations. However, it does not probe the nature of the interaction between fibers. Nevertheless, the presence of irreversibility in the unloading phase is a signature of frictional dissipation that accompanies local sliding at the contact points during the reorganization of the network.

Discussion

The study of structural and mechanical properties of aegagropilae allows us to draw a reliable scenario of their formation process. First, these seaballs are formed underwater without being reshaped during their transport or stay on the beach. They are mainly composed of smooth fibers produced by the decomposition of the seagrass *P. oceanica*. Second, the isotropic orientation of the fibers confirms that an aggregation mechanism takes place. Indeed, field observations suggest that aegagropilae are formed in submarine hollows, allowing for isotropic mixing and aggregation. This result is also in agreement with the measured log-normal distribution of mass, which is reminiscent of an aggregation or fragmentation process. Third, the density profile within a single seaball indicates that the dense outward shell is built on a compaction process. The small orthoradial excess in fiber orientation at the surface is also in favor of this chronology.

Notice that a compaction scenario on the basis of hydrodynamic forces (without collisions) is unlikely, because the magnitude of hydrodynamic forces is not sufficient to compact the aggregate. A possible mechanism that drives the compaction is repeated collisions of a seaball with the seabed. Let us estimate the deformation induced by this mechanism. When an elastic sphere of radius R, density ρ, Young modulus E, and Poisson ratio $\nu = 0$ impacts a rigid wall at a speed V, the maximum penetration $\delta_{\max}$ that it experiences is given in ref. 25:

$$\delta_{\max} = R\left(\frac{5\pi\rho V^2}{4E}\right)^{2/5}. \quad [7]$$

An estimation using $E \approx 10^5$ Pa, $R \approx 15$ mm, $\rho = 10^3$ kg m^{-3} (the density of a soaked seaball), and $V = 10$ cm s^{-1} (estimated from field observations; in agreement with the order of magnitude of the terminal velocity of a sinking seaball) yields $\delta_{\max} \approx 650$ μm. This value is of the same order of magnitude as the penetration for which we observed an irreversible deformation (Fig. 5). Therefore, collisions may induce the formation of an outward dense shell, which in turn, inhibits addition of material. The timescale for compaction should be small compared with the one for aggregation. Aggregation is indeed a long process because of the weak motion of water and root decomposition (which allows the fibers to be spatially localized), whereas compaction necessitates a stronger agitation induced by a sudden change in sea motion or seabed topography.

A thorough understanding of size distribution of such fiber network requires additional investigations. A fundamental issue is the effect of turbulence on the aggregation process and its saturation. Turbulent fluctuations take place at scales larger than the Kolmogorov scale, which can be a few millimeters in the ocean. The largest aegagropilae collected for this study have a major axis of approximately 9 cm, whereas the largest ever reported aegagropilae have a diameter around 20 cm. The existence of a maximal size raises the question of the influence of a surrounding turbulent flow on aggregation and fragmentation of objects of sizes in the inertial range of turbulence scales, whereas most of previous studies were dealing with sub-Kolmogorov flocs (31, 32).

Other than the peculiar application of seaballs, deriving a generic model that takes into account turbulent stress and fiber interactions inside the cluster would allow for a better understanding of floc formation in the paper industry and also, prevention of

this phenomenon in other applications. Finally, we showed that the weak forces that are at the origin of the compression of fiber network lead to a strong inhomogeneity of the density profile. This particular organization is probably at the origin of the surprisingly high stiffness of these seaballs. This feature may open perspectives to design materials with large weight to strain ratios.

ACKNOWLEDGMENTS. We thank the officials of Port-Cros National Park who allowed us to reach Porquerolles Island for this investigation; J. Chopin, E. Gouillart, and W. Woelffel for X-ray tomography; and A. Siria for SEM imaging. This work was partially funded by the PEPS AMPFi and carried out in the framework of Labex MEC Project ANR-10-LABX-0092 and A*MIDEX Project ANR-11-IDEX-0001-02 funded by the Investissements d'Avenir French Government program managed by Agence Nationale pour la Recherche.

1. Russell W (1893) Nouvelle note sur les pelotes marines. *Revue Générale de Botanique*, ed Klincksieck P (Librairie des Sciences Naturelles, Paris), Vol 5, pp 65–73. French.
2. Mathieson A, Dawes C (2002) *Chaetomorphia* balls foul New Hampshire, USA beaches. *Algae* 17:283–292.
3. Moyle J (1971) About beach balls. *Minn Volunteer* 34:38–41.
4. Alberts B, et al. (2002) *Molecular Biology of the Cell* (Garland Science, New York), 2nd Ed.
5. Janmey P, Amis E, Ferry J (1983) Rheology of fibrin clots. VI. Stress relaxation, creep, and differential dynamic modulus of fine clots in large shearing deformations. *J Rheol (NY NY)* 27:135–153.
6. Layton B, Sastry A (2004) A mechanical model for collagen fibril load sharing in the peripheral nerve of diabetic and non-diabetic rats. *J Biomech Eng* 126:803–814.
7. Nicholas A, Parra-Vasquez G, Duque JG, Green MJ, Pasquali M (2014) Assessment of length and bundle distribution of dilute single-walled carbon nanotubes by viscosity measurements. *AIChE J* 60:1499–1508.
8. Lundell F, Soderberg D, Alfredsson H (2011) Fluid mechanics of papermaking. *Annu Rev Fluid Mech* 43:195–217.
9. Hearle J, Grosberg P, Backer S (1969) *Structural Mechanics of Fibers, Yarns, and Fabrics* (Wiley Interscience, New York).
10. Chawla K (1998) *Fibrous Materials* (Cambridge Univ Press, Cambridge, UK).
11. Liu X, Wang X (2007) A comparative study on the felting propensity of animal fibers. *Text Res J* 77:957–963.
12. Parsa S, Calzavarini E, Toschi F, Voth G (2012) Rotation rate of rods in turbulent fluid flow. *Phys Rev Lett* 109:134501.
13. Brouzet C, Verhille G, Le Gal P (2014) Flexible fiber in a turbulent flow: A macroscopic polymer. *Phys Rev Lett* 112:074501.
14. Feller W (1971) *An Introduction to Probability Theory and Its Applications* (Wiley, New York), Vol 2.
15. Kolmogorov AN (1941) On the logarithmic normal distribution of particle sizes under grinding. *Dokl Akad Nauk SSSR* 31:99–101.
16. Koch A (1966) The logarithm in biology. 1. Mechanisms generating the log-normal distribution exactly. *J Theor Biol* 12:276–290.
17. Crow EL, Shimizu K, eds (1988) *Lognormal Distributions, Theory and Applications* (Marcel Dekker, Inc., New York).
18. Limpert E, Stahel W, Abbt M (2001) Log-normal distributions across the sciences: Keys and clues. *Bioscience* 51:341–352.
19. Straňák V, et al. (2011) Size-controlled formation of cu nanoclusters in pulsed magnetron sputtering system. *Surf Coat Technol* 205:2755–2762.
20. Soszynski R, Kerekes R (1988) Elastic interlocking of nylon fibers suspend in liquid. Part 1. Nature of cohesion among fibers. *Nord Pulp Pap Res J* 4:172–179.
21. Cannon J (1979) An experimental investigations of *Posidonia* balls. *Aquat Bot* 6:407–410.
22. Deboeuf S, Katzav E, Boudaoud A, Bonn D, Adda-Bedia M (2013) Comparative study of crumpling and folding of thin sheets. *Phys Rev Lett* 110:104301.
23. Cambou AD, Menon N (2011) Three-dimensional structure of a sheet crumpled into a ball. *Proc Natl Acad Sci USA* 108:14741–14745.
24. Courtois L, et al. (2012) Mechanical properties of monofilament entangled materials. *Adv Eng Mater* 14:1128–1133.
25. Landau LD, Lifshitz EM (1986) *Theory of Elasticity* (Pergamon, New York), 3rd Ed.
26. Greaves GN, Greer AL, Lakes RS, Rouxel T (2011) Poisson's ratio and modern materials. *Nat Mater* 10:823–837.
27. van Wyk C (1946) Note on the compressibility of wool. *J Text Inst* 37:T285–T292.
28. Poquillon D, Viguier B, Andrieu E (2005) Experimental data about mechanical behaviour during compression tests for various matted fibres. *J Mater Sci* 40:5963–5970.
29. Toll S (1998) Packing mechanics of fiber reinforcements. *Polym Eng Sci* 38:1337–1350.
30. Masse J, Salvo L, Rodney D, Brechet Y, Bouaziz O (2006) Influence of relative density on the architecture and mechanical behaviour of a steel metallic wool. *Scr Mater* 54:1379–1383.
31. Pumir A, Wilkinson M (2016) Collisional aggregation due to turbulence. *Annu Rev Condens Matter Phys* 7:141–170.
32. Bache DH (2004) Floc rupture and turbulence: A framework for analysis. *Chem Eng Sci* 59:2521–2534.